*Geophysical Prospecting*, 1996, 44, 499–523

# Practical techniques for 3D resistivity surveys and data inversion[1]

M.H. Loke[2] and R.D. Barker[3]

## Abstract

Techniques to reduce the time needed to carry out 3D resistivity surveys with a moderate number (25 to 100) of electrodes and the computing time required to interpret the data have been developed. The electrodes in a 3D survey are normally arranged in a square grid and the pole-pole array is used to make the potential measurements. The number of measurements required can be reduced to about one-third of the maximum possible number without seriously degrading the resolution of the resulting inversion model by making measurements along the horizontal, vertical and 45° diagonal rows of electrodes passing through the current electrode. The smoothness-constrained least-squares inversion method is used for the data interpretation. The computing time required by this technique can be greatly reduced by using a homogeneous half-space as the starting model so that the Jacobian matrix of partial derivatives can be calculated analytically. A quasi-Newton updating method is then used to estimate the partial derivatives for subsequent iterations. This inversion technique has been tested on synthetic and field data where a satisfactory model is obtained using a modest amount of computer time. On an 80486DX2/66 microcomputer, it takes about 20 minutes to invert the data from a 7 by 7 electrode survey grid. Using the techniques described below, 3D resistivity surveys and data inversion can be carried out using commercially available field equipment and an inexpensive microcomputer.

## Introduction

Although all geological structures are three-dimensional (3D) in nature, 3D resistivity surveys are carried out rarely at the present time compared to conventional one-dimensional (1D) resistivity sounding (Koefoed 1979) or even

---

[1] Paper presented at the 57th EAEG Meeting, May–June 1995, Glasgow, UK. Received November 1994, revision accepted August 1995.

[2] School of Physics, Universiti Sains Malaysia, 11800 Penang, Malaysia. (Email: mhloke@usm.my). Formerly at [3].

[3] School of Earth Sciences, The University of Birmingham, Birmingham B15 2TT, U.K. (Email: BARKER@ers.bham.ac.uk).

two-dimensional (2D) resistivity tomography (Griffiths and Barker 1993) surveys. This is probably due to the large number of field measurements needed for 3D surveys and the lack of suitable automatic inversion software. Significant progress has been made within the last decade in the development of field equipment and techniques for carrying out 2D resistivity tomography surveys (Griffiths, Turnbull and Olayinka 1990) and fast inversion algorithms to interpret the data (Loke and Barker 1996). A 2D model for the subsurface gives reasonably accurate results in areas with elongated geological structures. However, more complex structures (Park and Van 1991) can only be adequately represented by a 3D subsurface model.

Most current 3D resistivity inversion techniques are either approximate methods or they require powerful computing facilities. A one step inversion technique using the Born approximation was used by Li and Oldenburg (1992) to give a useful initial model for the subsurface. However, as indicated by the authors, it should be regarded as an initial model which can be further improved by using an iterative method. A fast iterative inversion technique using alpha centres has also been used (Petrick, Sill and Ward 1981). Since this technique uses an approximate method to calculate the model apparent resistivity values, the results are likely to be less accurate than a technique which uses the finite-element or finite-difference methods for the forward modelling calculations. The finite-element method was used by Shima (1992) to improve an initial model obtained by the alpha centres method. Park and Van (1991) used the finite-difference method and the total least-squares inversion method to invert the data obtained with a 5 by 5 rectangular grid of electrodes. Recently, Sasaki (1994) described the use of full and approximate 3D inversion methods using the finite-element method. The inversion techniques by Shima (1992), Park and Van (1991) and Sasaki (1994) were implemented on mainframe computers due to the large number of computations needed. However, such powerful computing resources are not conveniently available to small geophysical companies, particularly in third world countries. For the same reason, it would not be practical to carry out the data interpretation in the field during the course of a survey.

The two main problems in carrying out 3D surveys on a regular basis are the lack of suitable field equipment and the requirement of powerful computers to process the data. To overcome the first problem, we examine ways to adapt existing field equipment used for 2D surveys to carry out 3D surveys. To overcome the second problem, a fast 3D inversion program using a quasi-Newton optimization method (Broyden 1972) was developed which can be used on commonly available microcomputers.

In the next section, the field techniques are described. A brief description of the quasi-Newton inversion method is then given. This is followed by a discussion on ways to reduce the computing time required by the finite-difference method. Finally, two examples of the results obtained by the inversion program are given.

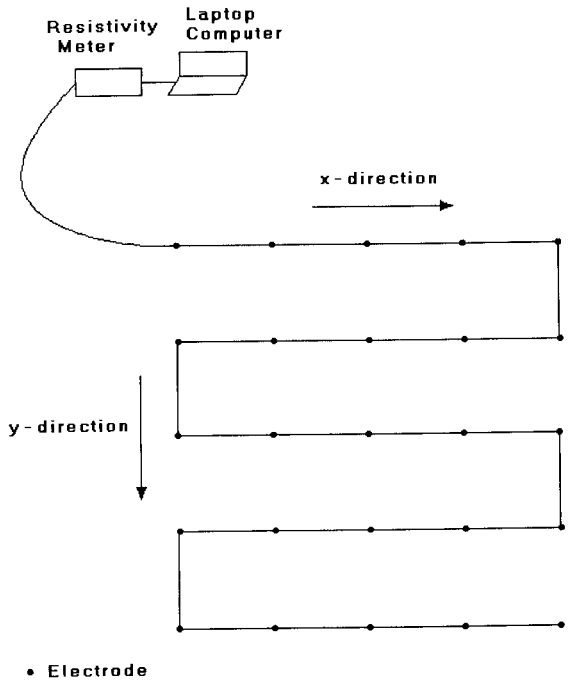


**Figure 1.** Arrangement of electrodes along a multicore cable for a 3D resistivity survey.

## Method

*3D field surveys*

Two-dimensional resistivity surveys are usually carried out with a computer-controlled multiplexer system with a number of electrodes connected to a multicore cable. One such system is the Campus Imager System where each electrode along the cable can be used as a current or potential electrode (Griffiths *et al.* 1990; Griffiths and Barker 1993). Our present interest is in 3D surveys using a moderate number (25 to 100) of electrodes which can be carried out with this type of field equipment. Figure 1 shows one possible arrangement of the electrodes for a 3D survey using a 25-electrode system. For convenience the electrodes are usually arranged in a square grid with the same unit electrode spacing in the $x$- and $y$-directions. In order to map slightly elongated bodies, a rectangular grid with different numbers of electrodes and spacings in the $x$- and $y$-directions could be used. The pole-pole electrode configuration is commonly used for 3D surveys, such as the E-SCAN method (Li and Oldenburg 1992). The maximum number of independent measurements $n_{max}$ that can be made with $n_e$ electrodes (Xu and Noel 1993) is given by

$$n_{max} = n_e(n_e - 1)/2.$$

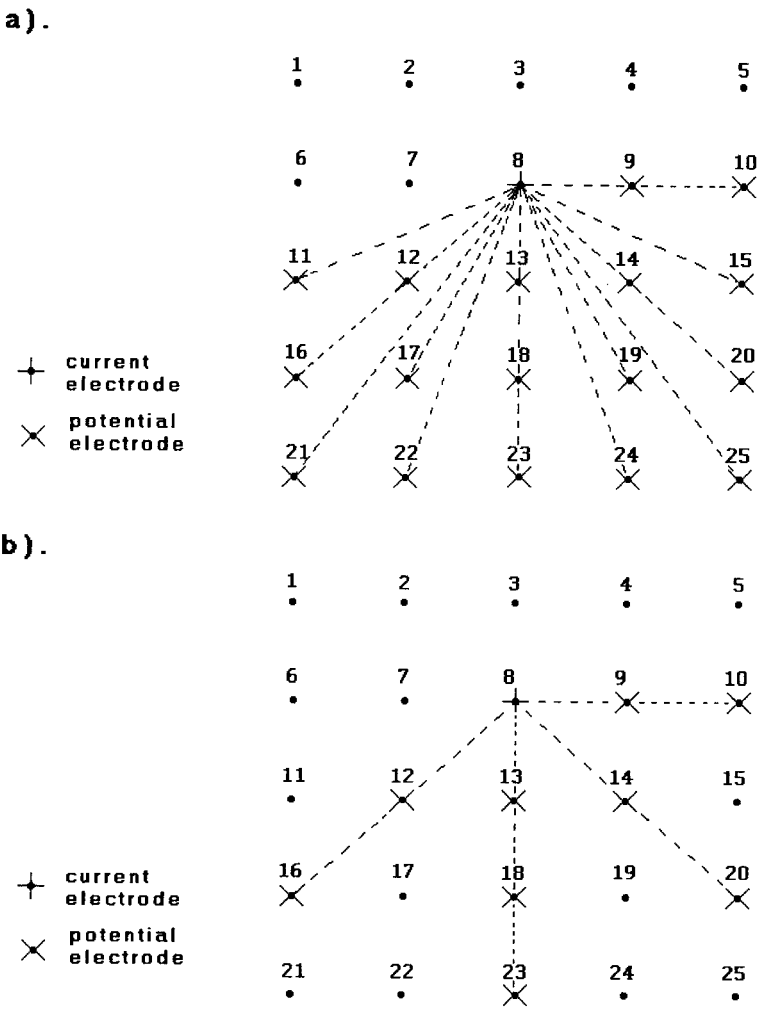


**Figure 2.** The location of potential electrodes corresponding to a single current electrode in the arrangement used by (a) a survey to measure the complete data set and (b) a cross-diagonal survey.

In this case, each electrode in turn is used as a current electrode and the potentials at all the other electrodes are measured. Note that because of reciprocity, it is only necessary to measure the potentials at the electrodes with a higher index number than the current electrode in Fig. 2a. For a 5 by 5 electrode grid, a complete data set (Xu and Noel 1993) will have 300 datum points. For 7 by 7 and 10 by 10 electrode grids, the numbers of measurements are 1176 and 4500 respectively. It can be very time-consuming to make such a large number of measurements with typical single-channel resistivity meters commonly used for 2D surveys. For example, it could take

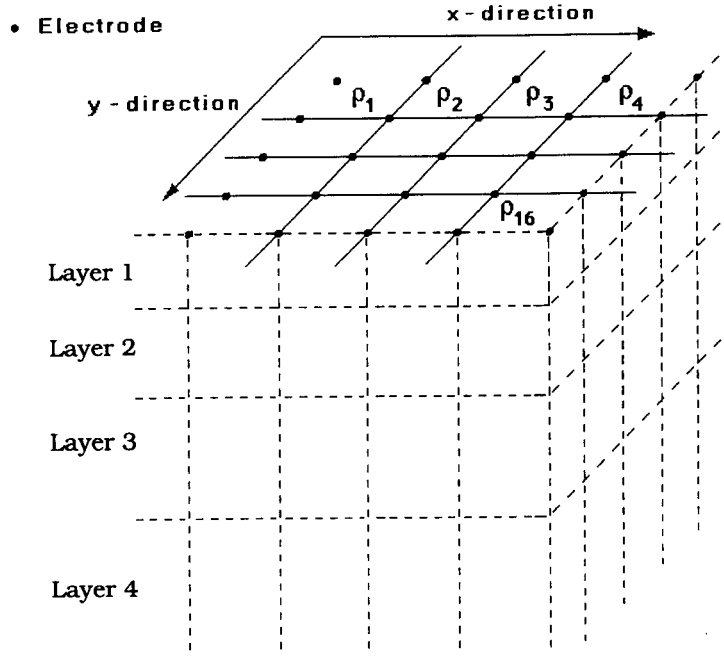


**Figure 3.** The arrangement of the blocks in the 3D model used. In calculating the apparent resistivity values and their partial derivatives, the blocks at the sides are extended horizontally sideways and the base of the bottom layer of blocks is extended downwards to the edges of the finite-difference mesh used.

several hours to make the 1176 measurements for a 7 by 7 survey grid with a standard low-frequency earth resistance meter, although speed is partly determined by the grid spacing and the magnitude of the measured resistances (Griffiths and Barker 1993). To reduce the number of measurements required without seriously degrading the quality of the model obtained, an alternative measurement sequence has been tested (Fig. 2b). In this proposed 'cross-diagonal survey' technique, the potential measurements are only made at the electrodes along the horizontal, vertical and the 45° diagonal lines passing through the current electrode. The number of datum points with this arrangement for a 7 by 7 grid is reduced to 476.

*Smoothness-constrained least-squares inversion method*

The 3D model used to interpret the data is shown in Fig. 3. The subsurface is divided into several layers and each layer is further subdivided into a number of rectangular blocks. The interior blocks within each layer have the same size. The blocks at the sides are extended horizontally sideways and the base of the bottom layer of blocks is extended downwards to the edges of the finite-difference mesh used to calculate

the apparent resistivity values. Note that the upper surfaces of the interior blocks in the topmost layer have an electrode at each corner. The thickness of the top layer is set at 0.70 times the unit electrode spacing used, which is slightly smaller than the median depth of investigation (0.87 times) of the pole-pole array for a homogeneous half-space (Edwards 1977). From a number of tests that were carried out, we have found that the inversion program could take a much longer time to converge if the thickness of the top layer is significantly less than 0.70 times the unit electrode spacing. If a thicker top layer is used, the near-surface resistivity variations are not well resolved. Since the resolution of the resistivity measurements decreases with depth, the thickness of each subsequent lower layer is increased by 15%. The number of layers in the model used is adjusted such that the depth to the top surface of the bottom layer is less than the median depth of investigation of the largest electrode spacing along a line of electrodes. As an example, for a 7 by 7 survey grid, the largest electrode spacing along the $x$- or $y$-direction is 6 times the unit electrode spacing used.

The smoothness-constrained least-squares method has been widely used in the inversion of geoelectrical data using 2D and 3D subsurface models (Sasaki 1989, 1994; deGroot-Hedlin and Constable 1990). The system of normal equations used in this method is given by

$$(\mathbf{J}_i^{\mathrm{T}}\mathbf{J}_i + \lambda_i \mathbf{C}^{\mathrm{T}}\mathbf{C})\mathbf{p}_i = \mathbf{J}_i^{\mathrm{T}}\mathbf{g}_i, \tag{1}$$

where $i$ is the iteration number, $\mathbf{J}_i$ is the Jacobian matrix of partial derivatives, $\mathbf{g}_i$ is the discrepancy vector which contains the differences between the logarithms of the measured and calculated apparent resistivity values, $\lambda_i$ is the damping factor and $\mathbf{p}_i$ is the perturbation vector to the model parameters for the $i$th iteration. The flatness filter $\mathbf{C}$ is used to constrain the smoothness of the perturbations to the model parameters to some constant value. The amplitudes of the elements of the flatness filter matrix $\mathbf{C}$ are increased by about 15% for each deeper row to stabilize the inversion process.

The smoothness-constrained least-squares method has proved to be a robust technique which converges rapidly. The main problem in using the conventional least-squares method on microcomputers for 2D and 3D problems is the time and memory space required to calculate the elements of the Jacobian matrix $\mathbf{J}_i$ using the finite-element or finite-difference method (Sasaki 1989; Park and Van 1991). Loke and Barker (1996) have overcome this problem in 2D resistivity inversion by using a homogeneous half-space as the starting model so that the partial derivatives can be calculated analytically. The partial derivative of the potential $\phi$ due to a change in the resistivity of a volume element $V$ in a homogeneous half-space with resistivity $\rho$ is given (Loke and Barker 1995) by

$$\frac{\partial \phi}{\partial \rho} = \frac{I}{4\pi^2}\int_V \frac{x(x-a) + y(y-b) + z^2}{(x^2+y^2+z^2)^{1.5}[(x-a)^2 + (y-b)^2 + z^2]^{1.5}}\,\mathrm{d}x\,\mathrm{d}y\,\mathrm{d}z, \tag{2}$$

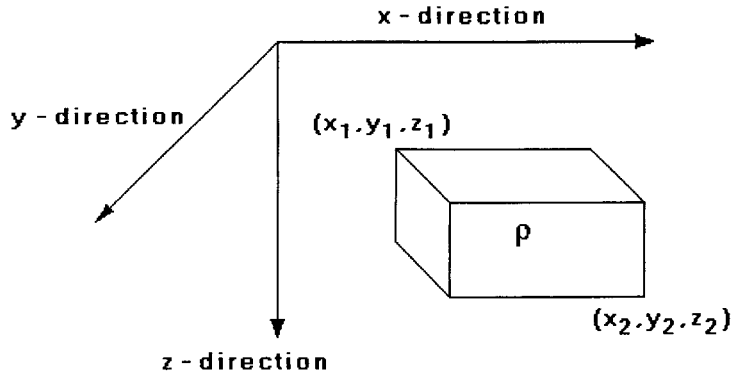


**Figure 4.** The parameters used in the calculation of the partial derivative for a single rectangular block within the 3D model used.

where the current source $I$ is located at the origin $(0,0,0)$ and the potential electrode is located at $(a,b,0)$. For a rectangular block in the model (Fig. 4), the above volume integral can be determined by using Gaussian quadrature (Churchhouse 1981) which uses the following approximation:

$$\frac{\partial\phi}{\partial\rho} \approx \frac{VI}{4\pi^2} \sum_{k=1}^{n_z} \sum_{j=1}^{n_y} \sum_{i=1}^{n_x} f_i f_j f_k \frac{u(u-\alpha)+v(v-\beta)+w^2}{(u^2+v^2+w^2)^{1.5}[(u-\alpha)^2+(v-\beta)^2+w^2]^{1.5}}, \tag{3}$$

where

$$u = (2x - x_1 - x_2)/(x_1 - x_2),$$
$$v = (2y - y_1 - y_2)/(y_1 - y_2),$$
$$\alpha = (2a - x_1 - x_2)/(x_1 - x_2),$$
$$\beta = (2b - y_1 - y_2)/(y_1 - y_2),$$
$$w = (2z - z_1 - z_2)/(z_1 - z_2),$$
$$V = 0.125(x_1 - x_2)(y_1 - y_2)(z_1 - z_2).$$

The top, left, back corner of the block is located at $(x_1, y_1, z_1)$ and the opposite corner is at $(x_2, y_2, z_2)$. The parameters $n_x$, $n_y$ and $n_z$ are the number of function evaluations in the $x$-, $y$- and $z$-directions respectively and $f_i$, $f_j$ and $f_k$ are the weights (corresponding to the values of $n_x$, $n_y$ and $n_z$ used) which are multiplied by the function values to obtain the value of the integral. Tables with the weights ($f$) and abscissae ($u$, $v$, $w$) for several values of function evaluations ($n$) may be found in Churchhouse (1981). When the rectangular block is next to the current or potential electrode, $n_x$, $n_y$ and $n_z$ are all set to 6 which gives a total of 216 function evaluations. The number of function evaluations in the $x$-, $y$- and $z$-directions are progressively reduced as the minimum distance of the block from either electrode increases. Since

the term within the triple summation in (3) only involves simple rational functions, each function evaluation can be calculated rapidly.

The method described above gives the partial derivative values for the starting homogeneous earth model. For subsequent iterations, the partials derivatives are estimated by using a quasi-Newton updating method (Bourji and Walker 1990). The Jacobian matrix $\mathbf{J}_i$ for the $i$th iteration is replaced by an approximation $\mathbf{B}_i$. The following updating equation by Broyden (1965) was used:

$$\mathbf{B}_{i+1} = \mathbf{B}_i + \mathbf{u}_i \mathbf{p}_i^{\mathrm{T}}, \tag{4}$$

where

$$\mathbf{u}_i = (\Delta \mathbf{y}_i - \mathbf{B}_i \mathbf{p}_i)/\mathbf{p}_i^{\mathrm{T}} \mathbf{p}_i,$$

$$\Delta \mathbf{y}_i = \mathbf{y}_{i+1} - \mathbf{y}_i,$$

and $\mathbf{y}_i$ is the model response for the $i$th iteration. The approximation of the Jacobian matrix $\mathbf{B}_{i+1}$ for the $(i+1)$th iteration is calculated using the Jacobian matrix approximation $\mathbf{B}_i$, the parameter perturbation vector $\mathbf{p}_i$ and the change in the model response $\Delta \mathbf{y}_i$ for the $i$th iteration. Since the updating matrix $\mathbf{u}_i \mathbf{p}_i^{\mathrm{T}}$ is a rank-one matrix, the time taken to solve the least-squares equation (1) can be substantially reduced by making use of matrix updating techniques (Golub and van Loan 1989; Loke and Barker 1996) associated with the numerical technique used to solve the least-squares equation.

*Optimizing the finite-difference method*

The potential distribution $\phi(\mathbf{x})$ due to a point current source $I(\mathbf{x}_S)$ is given by

$$\nabla \cdot [\sigma(\mathbf{x}) \nabla \phi(\mathbf{x})] = -I\delta(\mathbf{x} - \mathbf{x}_s), \tag{5}$$

where $\sigma(\mathbf{x})$ is the subsurface conductivity distribution. In the finite-difference method, the subsurface is discretized by using a rectangular mesh (Fig. 5) with irregular spacing of the nodes in the $x$-, $y$- and $z$-directions (Dey and Morrison 1979). We use a 3D mesh where the spacing between the nodes in the $x$- and $y$-directions in the central region of the mesh is one-half the smallest electrode spacing. Towards the sides and bottom of the mesh, the spacings between the nodes are progressively increased to simulate the 'infinitely distant' edges of the subsurface model. The rectangular elements within the mesh can have different conductivity values so that practically any subsurface distribution can be modelled by this method. The integrated finite-difference approach by Dey and Morrison (1979), which calculates the volume integral of (5) around each node, leads to the following matrix equation:

$$\mathbf{A}\phi = \mathbf{s}, \tag{6}$$

where the capacitance matrix $\mathbf{A}$ is a septadiagonal, positive definite symmetric matrix. The elements of this matrix depend only on the geometry and conductivity

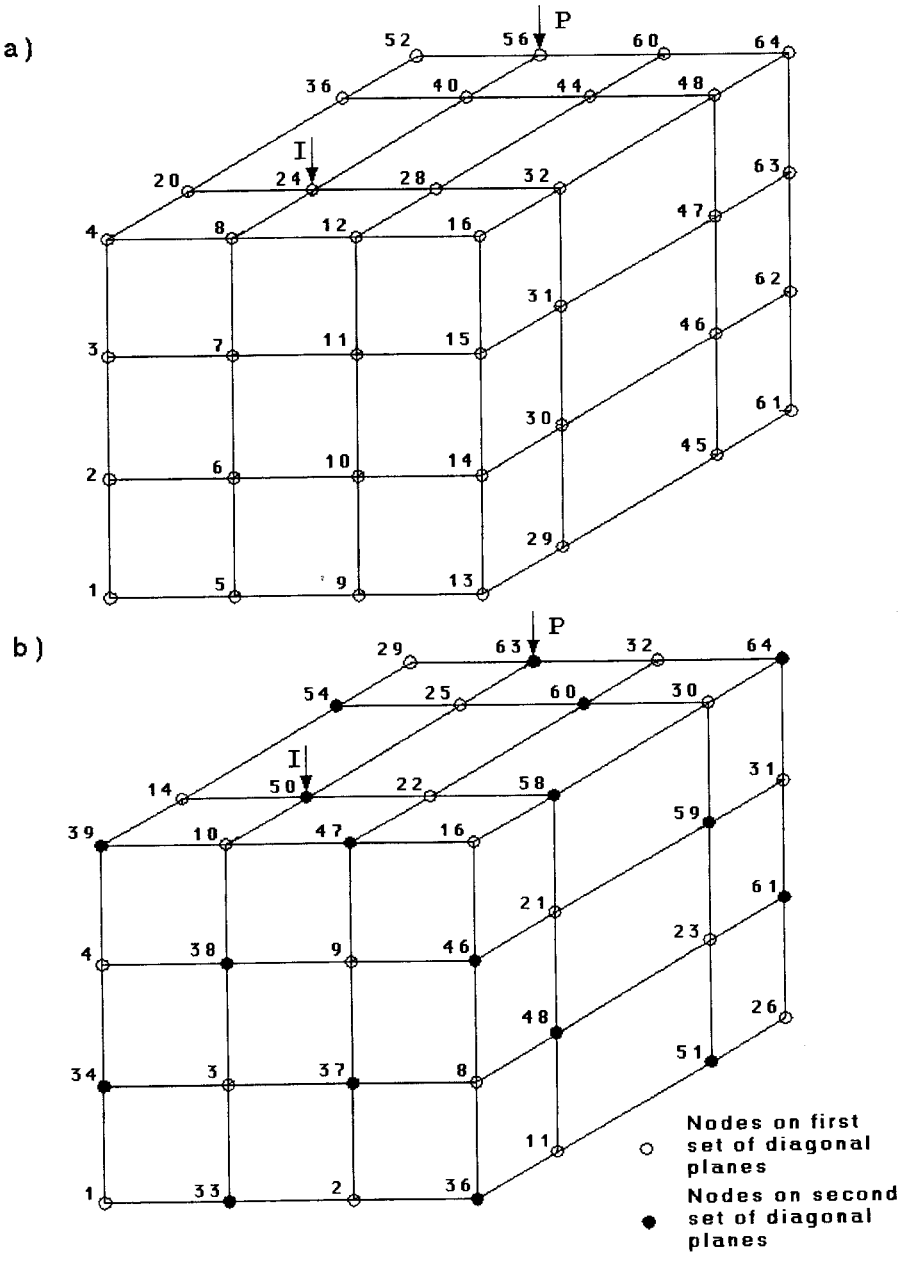


**Figure 5.** Finite difference grid with (a) natural column-by-column ordering and (b) alternate-plane ordering of the nodes.

**Table 1.** Comparison of memory required by band-Cholesky with natural column-by-column nodes ordering and the alternate-plane ordering using a general sparse matrix storage system. The memory ratio gives the ratio of the memory required by the alternate-plane ordering compared to the band method.

| Electrode configuration | Mesh size | Total number of nodes | Memory required in kilobytes | | Memory Ratio |
|---|---|---|---|---|---|
| | | | Band method | Alternate-plane | |
| 5 by 5 | 23 × 23 × 9 | 4761 | 3868.3 | 1510.8 | 0.39 |
| 7 by 7 | 27 × 27 × 11 | 8019 | 9335.8 | 3483.5 | 0.37 |
| 10 by 10 | 33 × 33 × 13 | 14157 | 23779.3 | 8584.2 | 0.36 |

distribution within the grid, and it does not depend on the current source vector **s**. The vector $\phi$ contains the potentials at the nodes. The most convenient method to calculate all the possible apparent resistivity measurements for the electrode arrangement shown in Fig. 2 is to calculate the potential distribution due to a single current electrode at each of the electrode locations. This means that for a 5 by 5 survey grid, it is necessary to solve the capacitance matrix equation (6) to determine the potential vectors for 24 different current source vectors. For such a large number of different current source vectors, it might be faster to use a direct method (rather than an iterative method) to solve the capacitance matrix equation (Dey and Morrison 1979). A commonly used direct method is the band-Cholesky technique (Martin and Wilkinson 1965) which first carries out the decomposition

$$\mathbf{A} = \mathbf{R}^{\mathrm{T}}\mathbf{R}. \tag{7}$$

The above decomposition is only carried out once for a single subsurface model. In order to determine the potential vector $\phi$ for each current source vector **s**, (7) is first solved by using the forward substitution step

$$\mathbf{R}^{\mathrm{T}}\mathbf{q} = \mathbf{s}, \tag{8}$$

followed by the backward substitution step

$$\mathbf{R}\phi = \mathbf{q}. \tag{9}$$

The time taken for the forward substitution step can be greatly reduced by taking advantage of the sparsity of the current source vector **s**. The time taken by the backward substitution step can be reduced by obtaining a partial solution of the potential vector $\phi$ (Loke and Barker 1996). As an example, Fig. 5a shows the nodes in a 4 × 4 × 4 finite-difference mesh. If the current electrode is at node 24, then the first 23 elements of the **s** vector are zero. It is only necessary to carry out the forward substitution steps for nodes 24 to 64 since the first 23 elements of the **q** vector in (8) are equal to zero. If the potential electrode is at node 56 (Fig. 5a), it is only necessary to carry out the back substitution step for nodes 64 to 56. Note that to calculate the apparent resistivity values, it is only necessary to determine the potentials at the nodes with the electrodes. However, if the partial derivatives are

directly calculated with the finite-difference method, it would be necessary to calculate the potentials at all the nodes.

The main disadvantage of using a direct method for solving the capacitance matrix equation for 3D problems is the huge amount of memory needed compared to iterative methods. The amount of memory needed depends on the number of nodes in the 3D mesh used. The total number of nodes depends on the number of nodes per unit electrode spacing. In general, a finer mesh will result in more accurate potential values calculated by the finite-difference method. Dey and Morrison (1979) used a mesh with four nodes between adjacent electrodes, while Park and Van (1991) used only one node per unit electrode spacing. We used a mesh with two nodes per unit electrode spacing in an attempt to strike a balance between reducing the memory required and the errors in the calculated potential values. The resulting finite-difference meshes used to model the data for three different survey electrode configurations are shown in Table 1 which also shows the computer memory required by the band-Cholesky method (Martin and Wilkinson 1965). About 23 megabytes of memory would be needed to model the data from a 10 by 10 electrode survey grid! Thus we have examined the use of sparse matrix techniques (George and Liu 1981) to reduce the memory needed to a more manageable level. Sparse matrix methods basically attempt to reduce the number of non-zero elements in the Cholesky decomposition matrix $\mathbf{R}$ in (7) by permuting the ordering of the node numbers in the mesh. Figure 5a shows the 'natural' ordering for a $4 \times 4 \times 4$ rectangular mesh used for the band-Cholesky method.

One simple but effective method widely used for 2D finite-difference rectangular grids is the 'black-red' or alternate-diagonal ordering (Woo *et al.* 1976). A 3D version of this type of ordering is shown in Fig. 5b where the nodes are separated into two sets of diagonal planes. The neighbouring nodes around any node lie on a different set of diagonal planes. The total memory required for the finite-difference mesh using the alternate-plane ordering is also listed in Table 1. To store the non-zero elements of the $\mathbf{R}$ matrix, the general sparse matrix allocation scheme described by Eisenstat, Schultz and Sherman (1976) and George and Liu (1981) is used. The total storage required by the alternate-plane ordering is less than 40 % of that required by the band method.

The time required by the forward and backward substitution steps in (8) and (9) can be further reduced by carefully organizing the location of the nodes with the electrodes so that they end up with larger node numbers. For the alternate-plane ordering system, this can be achieved by placing the nodes with the electrodes on the second set of diagonal planes. As an example, the node numbers for the current and potential electrodes in Fig. 5b have been increased to 50 and 63 respectively (compared to 24 and 56 in Fig. 5a) which reduces the time required by the substitution steps by more than half. The computer time and memory required can be further reduced by making use of more sophisticated sparse matrix ordering techniques such as the nested dissection and one-way dissection techniques (George and Liu 1981).

**Table 2.** Parameters of rectangular blocks test model. The resistivity of the surrounding medium is 10 Ω m.

| Block | *x*-dimensions m. | *y*-dimensions m. | *z*-dimensions m. | Resistivity Ω m |
|---|---|---|---|---|
| Upper | 1.0 to 5.0 | 1.0 to 2.0 | 0.0 to 0.70 | 100 |
| Lower | 1.0 to 4.0 | 2.0 to 5.0 | 0.70 to 2.43 | 1 |

On the 80486DX2/66 microcomputer, the finite-difference subroutine took about 42 s to calculate all the possible potential measurements for a 5 by 5 survey grid, and about 159 s for a 7 by 7 survey grid. The decomposition and solution steps took about 59% and 36% respectively of the total time. The remaining 5% of the total time was used in setting up the sparse matrix array structures and calculating the elements of the capacitance matrix. To check the accuracy of the finite-difference program, we used a two-layer test model where the resistivities of the top and bottom layers are 10.0 and 1.0 Ω m respectively. The thickness of the top layer is 1.51 m and the unit electrode spacing is 1.0 m. The potential values for the pole-pole array were compared with those calculated using the method described by Mooney *et al.* (1966) which has an accuracy of 0.1%. The maximum error in the potential values calculated by the finite-difference method was found to be about 4% for this test model.

*The inversion algorithm*

Since we use an algorithm similar to that described in detail by Loke and Barker (1996), only a very brief description is given here. The resistivity of the starting homogeneous earth model is calculated by taking the average of the logarithms of the measured apparent resistivity values. An initial damping factor $\lambda_0$ and a minimum damping factor $\lambda_m$ for the least-squares method is then selected. From a number of tests carried out with synthetic and field data sets, we have found that values of 0.20 and 0.03 for $\lambda_0$ and $\lambda_m$ usually give satisfactory results. However, in the computer program used, the damping factor values could be changed by the user if necessary. In each iteration, the change in the model resistivity values and Jacobian matrix are calculated using (1) and (4). After the first two iterations, the damping factor $\lambda$ is reduced by half if it is still larger than the minimum damping factor $\lambda_m$ selected. If the inversion process fails to reduce the apparent resistivity root-mean-square (rms) error, a line search using quadratic interpolation is first used to find the optimum step size for the model perturbation vector (Daniels 1978). If this also fails to reduce the rms error, the damping factor is increased. The inversion process is usually stopped when the relative change in the rms error is less than 5% (Loke and Barker 1996), or when the maximum number of iterations (usually about 10) is reached. Although a relatively simple algorithm is used, it has given satisfactory results for the computer generated and field data sets that we have used. However,

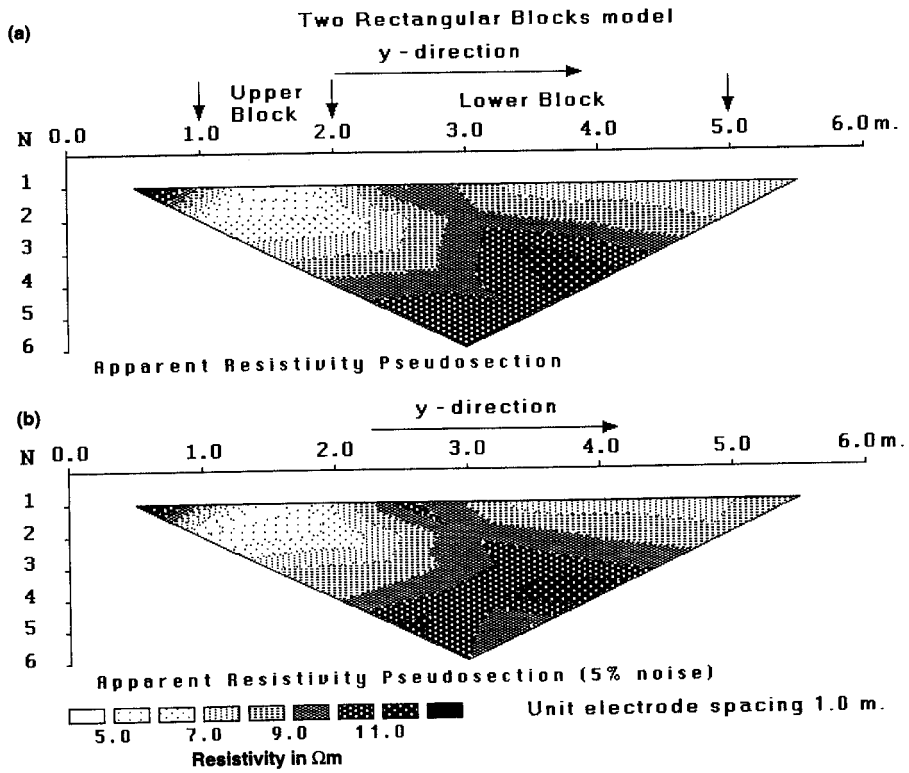


**Figure 6** (a) Apparent resistivity pseudosection along the line of electrodes at $x = 3.0$ m for the test model with two rectangular blocks in a homogeneous medium. (b) The apparent resistivity pseudosection obtained after adding 5% random noise to the data.

for some data sets, better results might be obtained by using a more sophisticated inversion algorithm (Dennis and Schnabel 1983).

## Results

We present the results obtained from the inversion of a synthetic data set and a field data set. For the synthetic data set, the models obtained using the complete data set and the reduced data set using the cross-diagonal survey technique are shown. All the calculations were carried out on an 80486DX2/66 microcomputer with 20 megabytes of memory.

### *Example 1: two rectangular blocks*

This model consists of two rectangular blocks of resistivities 100 Ω m and 1 Ω m embedded in a homogeneous half-space with a resistivity of 10 Ω m. The parameters of the rectangular blocks are listed in Table 2. The survey grid consists of a 7 by 7

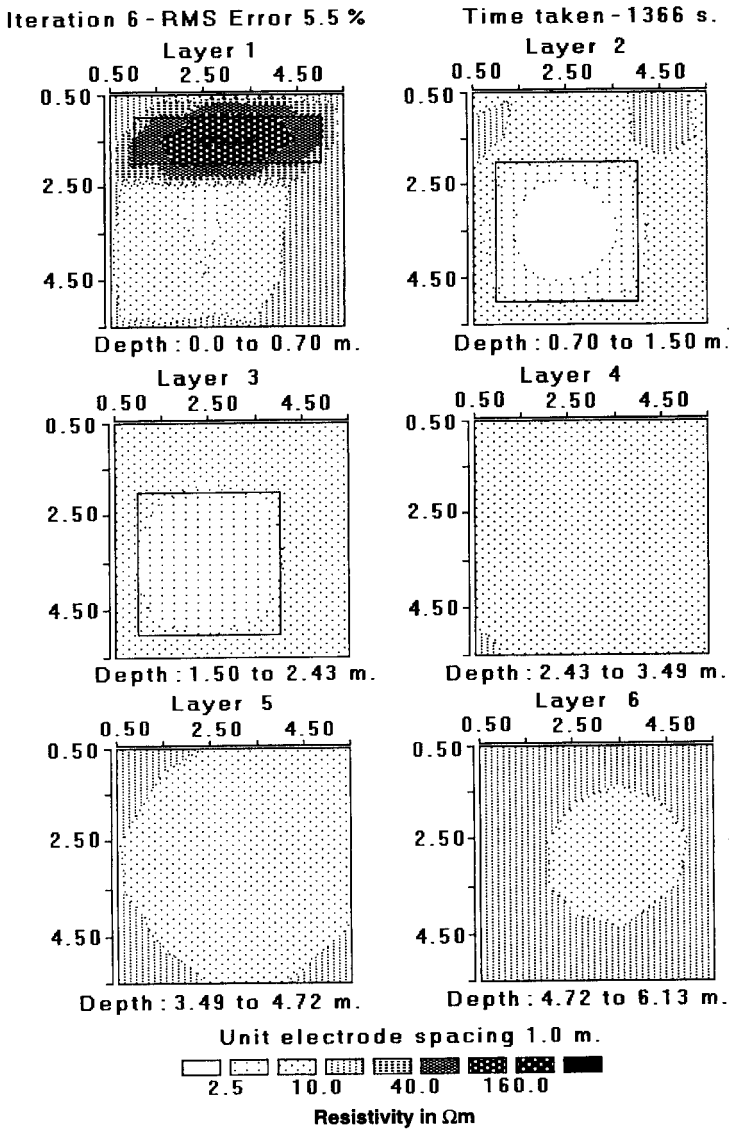


**Figure 7.** The model obtained from the inversion of the rectangular blocks model complete data set (with 1176 datum points) with 5% noise after 6 iterations. Note that in the true model, the upper block is confined to the top layer while the lower block is confined to the second and third layers. The outlines of the rectangular blocks are also shown for comparison.

grid with a unit electrode spacing of 1.0 m. The apparent resistivity values for all the possible pole–pole combinations were calculated using the finite-difference program. Figure 6a shows the pole-pole apparent resistivity pseudosection along the line of electrodes at $x$ equal to 3.0 m (i.e. in the $y$–$z$ plane) which cuts across both rectangular

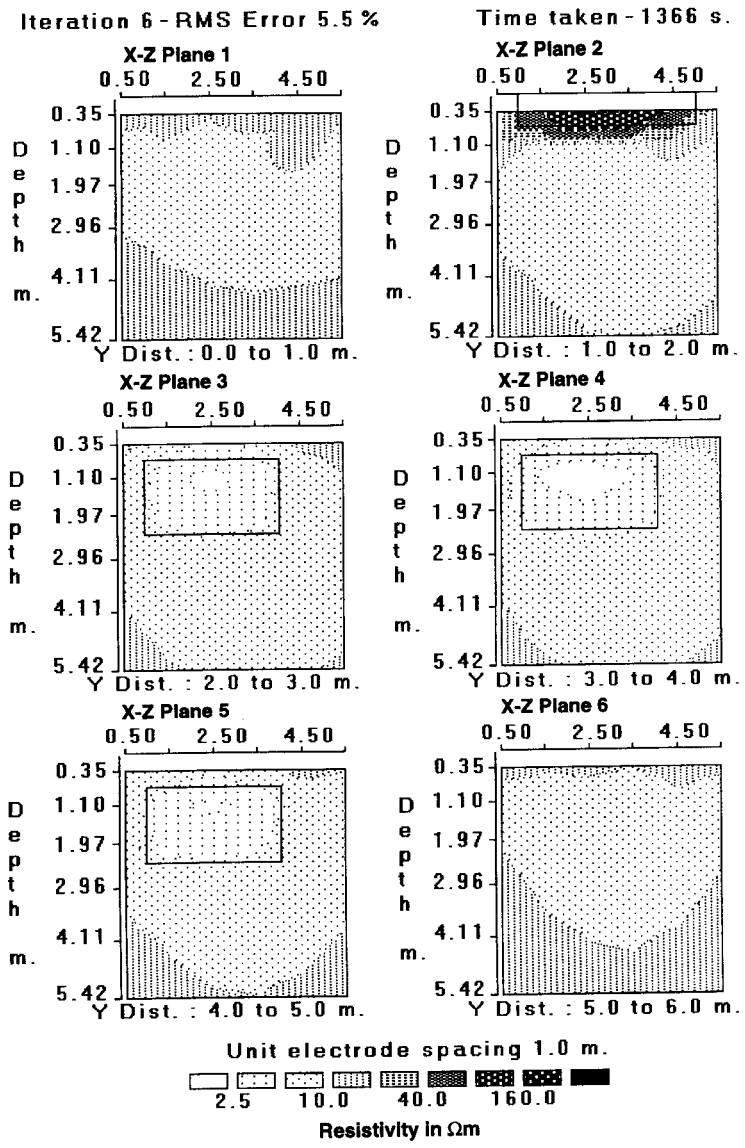


**Figure 8.** Vertical cross-sections of the model obtained from the inversion of the complete data set with 1176 datum points for the rectangular blocks model.

blocks. The upper high resistivity rectangular block causes a prominent low resistivity anomaly at the first datum level (corresponding to an electrode spacing of 1.0 m) which is flanked by two linear slanting high resistivity anomalies. This model shows an example of the 'anomaly inversion' phenomenon frequently observed in borehole logs where a body with a higher resistivity than the surrounding medium results in lower

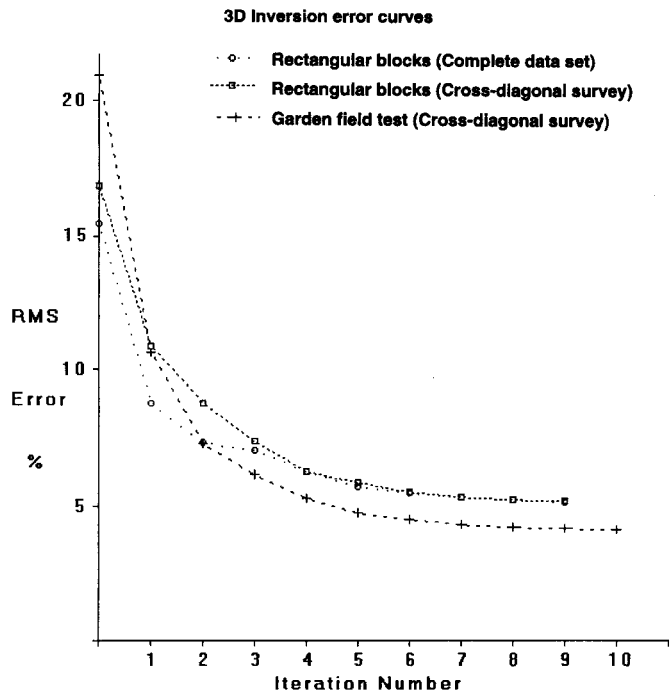


**Figure 9.** Change of the rms error with iteration number for the inversion of the two data sets for the rectangular blocks model, and for the inversion of the Birmingham field survey data.

apparent resistivity values when it has dimensions smaller than the electrode spacing. The anomaly of the upper block is superimposed on the anomaly caused by the lower block on the lower right side of the pseudosection. Due to the complex and overlapping anomalies produced by the two blocks, a simple inspection of the apparent resistivity pseudosection would not be sufficient to obtain an accurate picture of the true subsurface resistivity distribution.

In order to test the possible behaviour of the inversion method on field data, 5% random noise (Press *et al.* 1988) was added to the apparent resistivity data which caused some distortion of the pseudosection. The result is shown in Fig. 6b. The inversion model used consists of 216 rectangular blocks. The subsurface is divided into 6 layers and each layer is subdivided into 36 blocks. In the model obtained at the 6th iteration from the inversion of this data set (Fig. 7), the upper rectangular block is clearly shown. The lower rectangular block shows up as a region of low resistivity (less than 5 $\Omega$ m) in the 2nd and 3rd model layers. Figure 8 shows the vertical cross-sectional plots (along the $x$–$z$ plane) of the inverse model. The sides of the upper rectangular block are well resolved. The boundaries of the lower block are not as well resolved but the model shows the correct location and approximate size of the block. The change in the apparent resistivity rms error with iteration number is shown in Fig. 9. The initial homogeneous earth model has a rms error of about 15.5% which

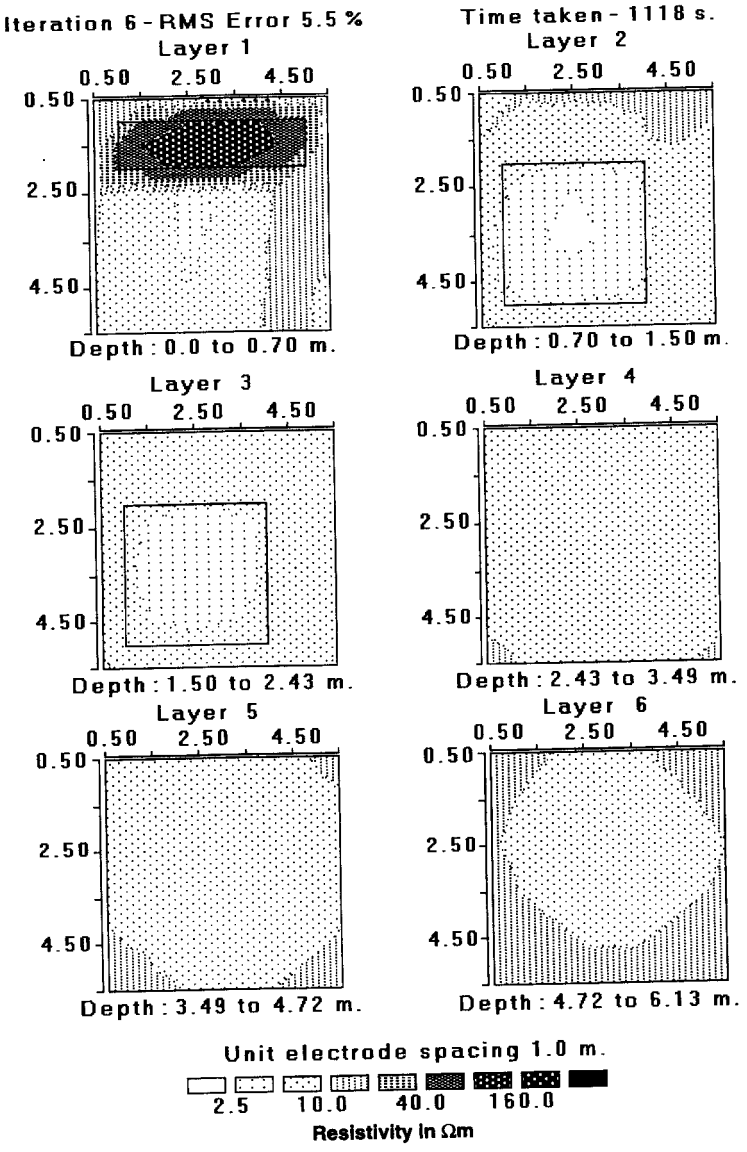


**Figure 10.** Horizontal cross-sections of the model obtained from the inversion of the rectangular blocks cross-diagonal survey data set with 5% noise after 6 iterations.

reduced to 5.2% after 9 iterations. The largest decrease in the rms error occurs in the first few iterations. The inversion process would normally be stopped at the 6th iteration since there is only a small change in the rms error after the 5th iteration.

The horizontal and vertical sections of the model obtained from the inversion of the cross-diagonal survey data set are shown in Figs 10 and 11. The results are similar

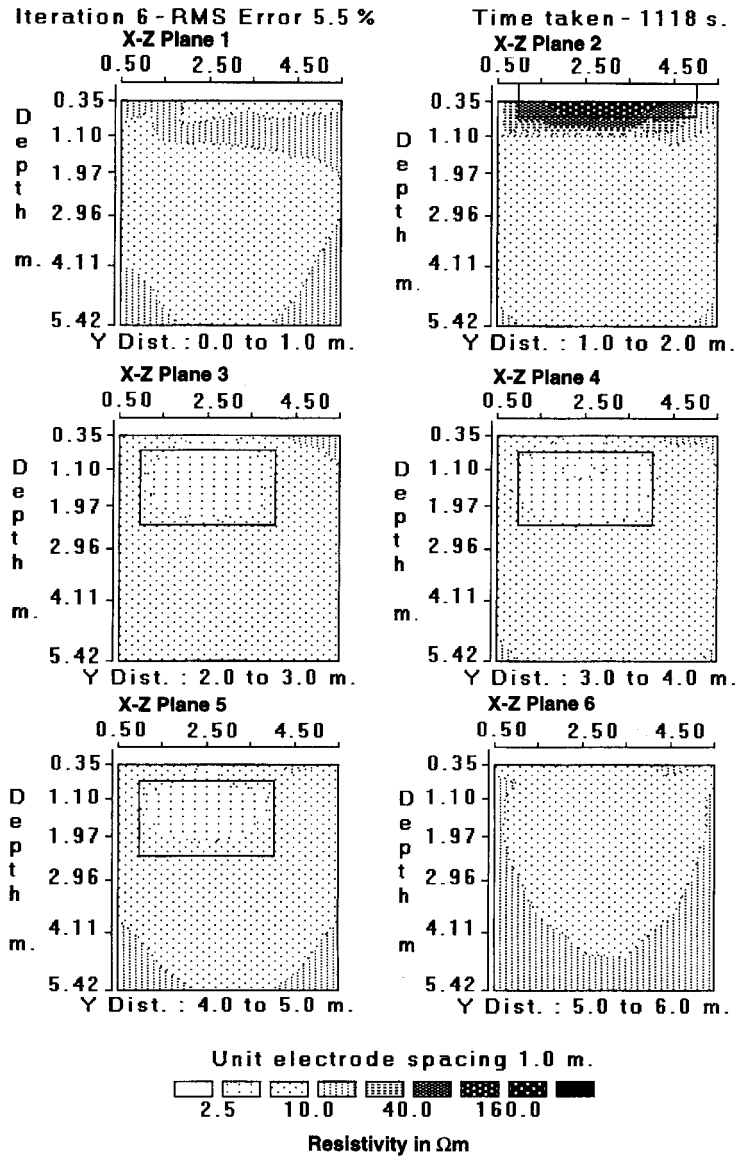


**Figure 11.** Vertical cross-sections of the model obtained from the inversion of the cross-diagonal survey data set for the rectangular blocks model.

to those obtained from the inversion of the complete data set (Figs 7 and 8). The upper block is well resolved. The lower block in the complete data set model (Fig. 8) is slightly sharper than in the cross-diagonal survey model (Fig. 11). The minimum resistivity value near the centre of the lower block (at the 6th iteration) is 1.3 Ω m in Fig. 8 compared to 2.0 Ω m in the cross-diagonal survey model. This is not surprising

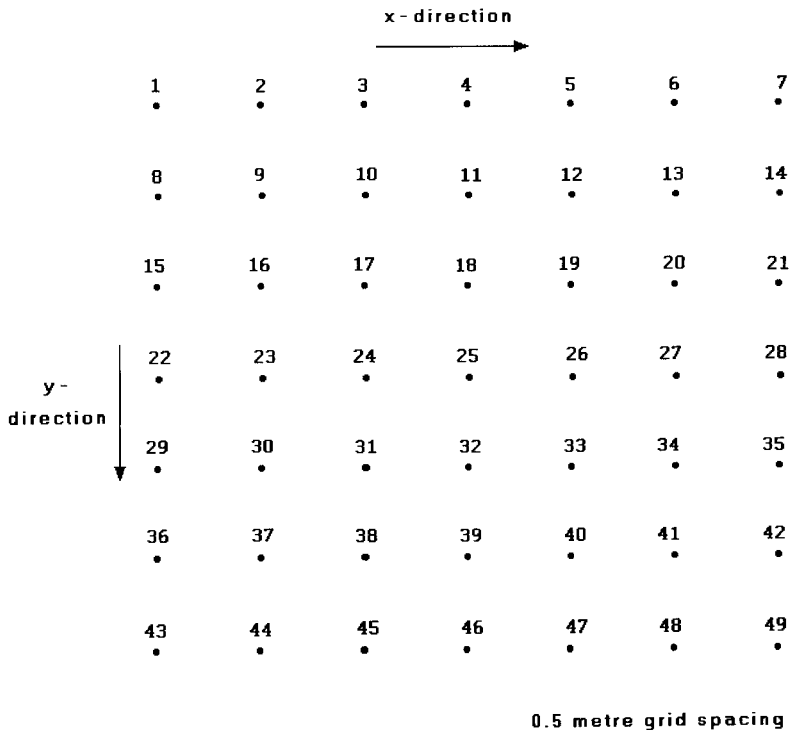


**Figure 12.** Schematic diagram of the arrangement of the electrodes in the Birmingham field survey test.

since the cross-diagonal survey uses only 476 datum points compared to 1176 points in the complete data set. In many situations, the slight reduction in the model resolution is more than offset by the large reduction in the field survey time required. The error curve for the inversion of the cross-diagonal survey data set shows a trend (Fig. 9) similar to that from the inversion of the complete data set.

It took about 20 minutes to obtain a satisfactory model in the inversion of both data sets. Loke and Barker (1996) have shown that in the 2D inversion of resistivity data there were no significant differences between the models obtained by the quasi-Newton and the conventional least-squares methods. However, the computer time and memory required by the quasi-Newton method to produce a satisfactory model is about an order of magnitude smaller. We have not attempted to carry out a direct comparison between the two methods for 3D resistivity inversion because of the large amount of computer time and memory that would be required by the conventional least-squares method.

*Example 2: Birmingham field test survey*

This field test was carried out in the Moseley area of Birmingham using a multi-

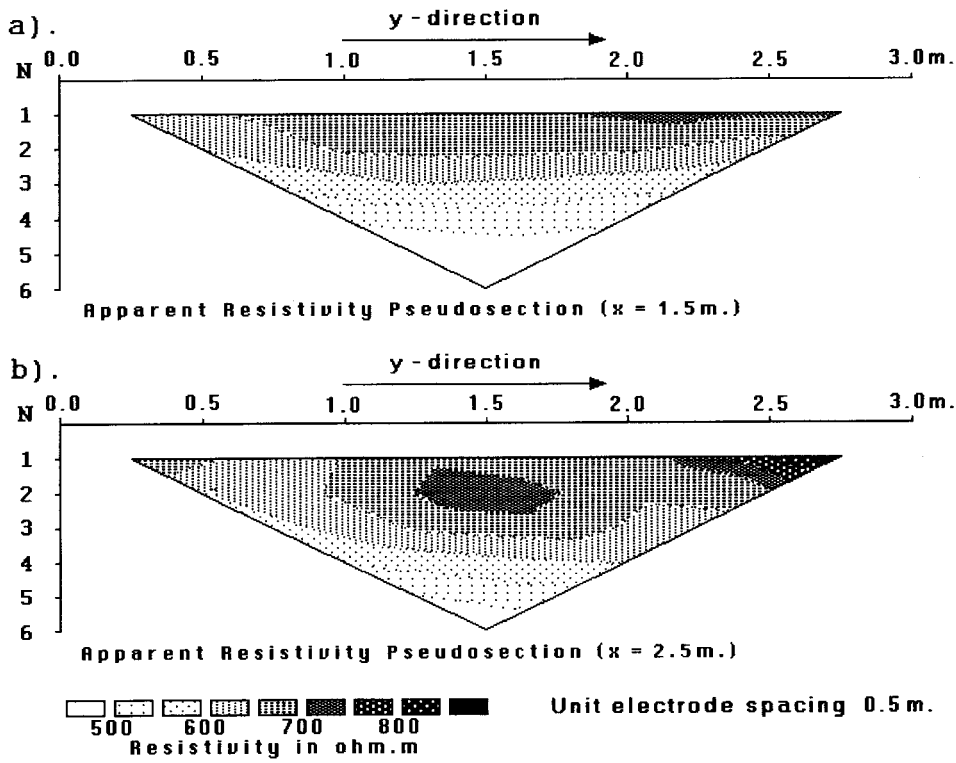


**Figure 13.** (a) Birmingham field survey apparent resistivity pseudosections along the line of electrodes at $x = 1.5$ m and at (b) $x = 2.5$ m.

electrode system with 50 electrodes commonly used for 2D resistivity surveys (Griffiths and Barker 1993). The electrodes are arranged in a 7 by 7 square grid with a unit electrode spacing of 0.5 m. There was a large sycamore tree just outside the survey area (Fig. 12). The two far electrodes were placed at more than 25 m from the grid to reduce their effects on the measured apparent resistivity values. The cross-diagonal survey technique was used to reduce the survey time. Figure 13 shows the pole–pole apparent resistivity pseudosections along the line of electrodes at $x$ equal to 1.5 m (across the middle of the survey area) and at $x$ equal to 2.5 m. There are significant differences between the two pseudosections although they are only 1 m apart. The subsurface is known to be highly inhomogeneous, consisting of sands and gravels.

The error curve for the inversion of this data set is also shown in Fig. 9. The program converged in about 6 iterations after which there is only a small change in the rms error. Figure 14 shows the horizontal sections of the model obtained at the 6th iteration. The two high resistivity zones in the upper left quadrant and the lower right corner of Layer 2 are probably gravel beds. The two low-resistivity linear features in Layer 1 near the lower edge of the survey area could be due to roots from

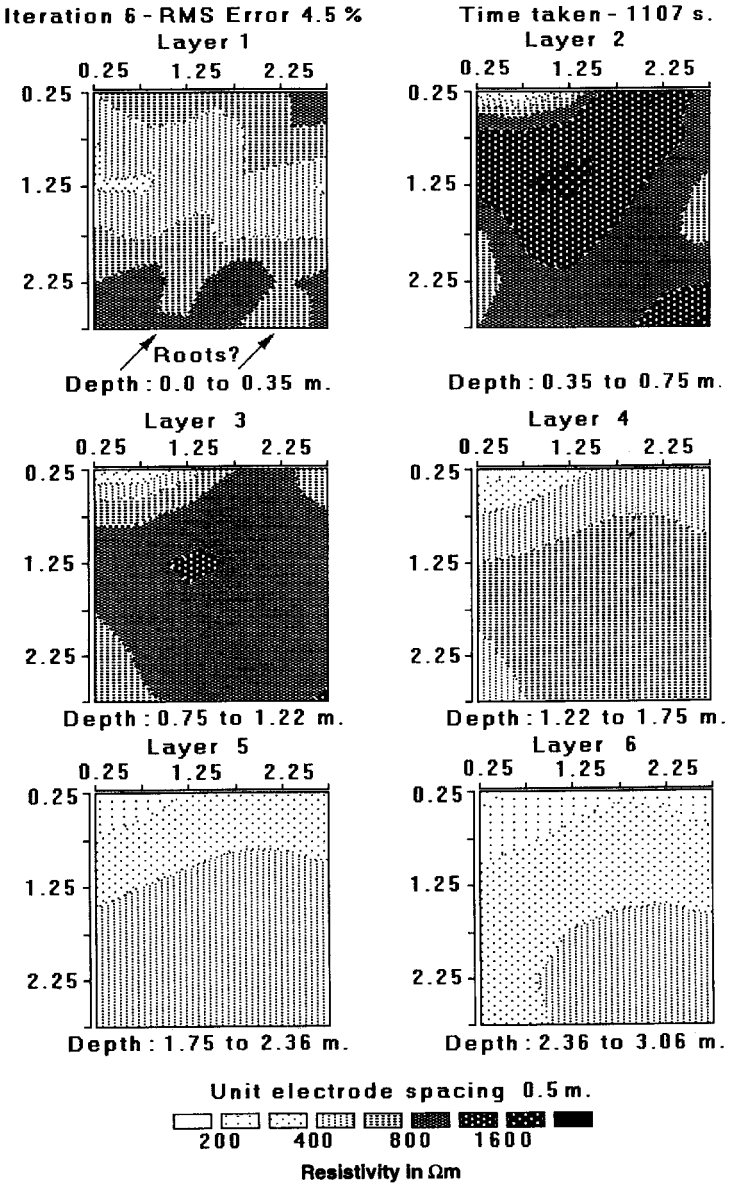


**Figure 14.** Horizontal cross-sections of the model obtained from the inversion of the Birmingham field survey data set.

the sycamore tree (Fig. 12). The vertical extent of the gravel beds is more clearly shown in the vertical cross-sections across the model (Fig. 15). The inverse model shows that the subsurface resistivity distribution is highly inhomogeneous and can change rapidly within a short distance. In such a situation a simpler 2D resistivity

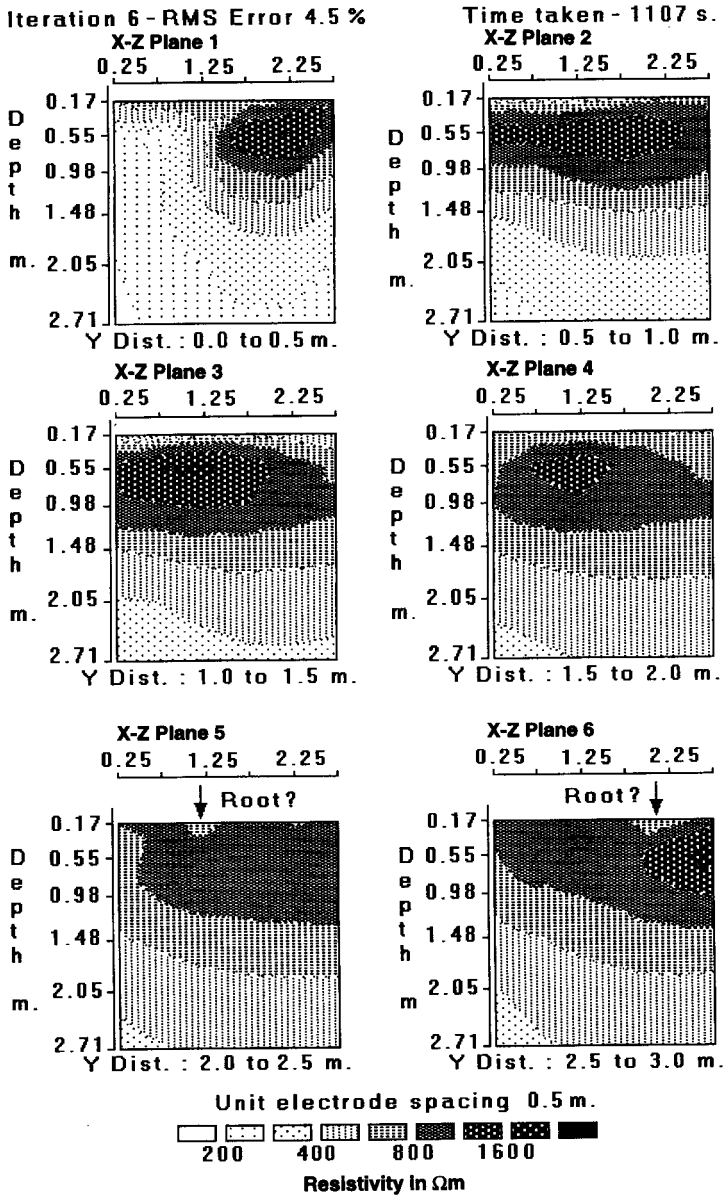


**Figure 15.** Vertical cross-sections of the model obtained from the inversion of the Birmingham field survey data set.

model (and certainly a 1D model from conventional sounding surveys) would probably not be sufficiently accurate.

## Conclusions

We have presented a field technique and an inversion method which enable 3D resistivity surveys and data interpretation to be carried out using commercially available resistivity field equipment and inexpensive microcomputers. The field survey time required can be greatly reduced by using the cross-diagonal survey technique at the cost of a slight reduction in the model resolution. A fast inversion technique using a quasi-Newton optimization method has been developed for the automatic inversion of 3D resistivity data. In the tests carried out with synthetic and field data, the quasi-Newton inversion method has proved to be a robust technique which converges rapidly. This inversion method is able to resolve complex 3D geological structures in situations where a 2D resistivity survey and inversion is not adequate. The inversion of a single data set from a 7 by 7 survey grid takes about 20 minutes on an 80486DX2/66 microcomputer.

Research is being carried out into different ways to improve further the inversion method by using more sophisticated schemes to determine the optimum damping factor and step size for the model perturbation vector (deGroot-Hedlin and Constable 1990), other, possibly better, quasi-Newton updating techniques (Dennis and Schnabel 1983) and by normalizing the $\mathbf{J}^{\mathrm{T}}\mathbf{J}$ matrix (Lines and Treitel 1984). Research is also being carried out on the use of sparse least-squares techniques (Bjorck 1972) to reduce the computer time and memory required to solve the least-squares equation. Newer microcomputers based on the Intel Pentium microprocessor are about 5 to 10 times faster than the 80486DX2/66 computer used in this research. Thus it should be possible to carry out the inversion of data from larger survey grids (e.g. 14 by 14) on commonly available microcomputers. The main obstacle to carrying out surveys with such large grids is probably the time needed to make the field measurements using conventional single-channel resistivity meters. A multichannel resistivity meter would probably be required to carry out such surveys within a reasonable amount of time.

## Acknowledgements

M.H.L. thanks The Association of Commonwealth Universities and Universiti Sains Malaysia for the scholarship provided. We also thank two anonymous reviewers and Prof. D. Oldenburg for critical reviews and comments.

## References

Bjorck A. 1972. Methods for sparse linear least squares problems. In: *Sparse Matrix Computations* (eds J.R. Bunch and D.J. Rose), pp. 177–200. Academic Press, Inc.

Bourji S.K. and Walker H.F. 1990. Least-change secant updates of nonsquare matrices. *SIAM Journal of Numerical Analysis* **27**, 1263–1294.

Broyden C.G. 1965. A class of methods for solving nonlinear simultaneous equations. *Mathematics of Computation* **19**, 577–593.

Broyden C.G. 1972. Quasi-Newton methods. In: *Numerical Methods for Unconstrained Optimization* (ed. W. Murray), pp. 87–106. Academic Press, Inc.

Churchhouse R.F.(ed.) 1981. *Handbook of Applicable Mathematics. Vol. III: Numerical Methods*. John Wiley & Sons, Inc.

Daniels R.W. 1978. *An Introduction to Numerical Methods and Optimization Techniques*. Elsevier Science Publishing Co.

deGroot-Hedlin C. and Constable S.C. 1990. Occam's inversion to generate smooth, two-dimensional models from magnetotelluric data. *Geophysics* **55**, 1613–1624.

Dennis J.E. and Schnabel R. 1983. *Numerical Methods for Unconstrained Optimization and Nonlinear Equations*. Prentice–Hall, Inc.

Dey A. and Morrison H.F. 1979. Resistivity modeling for arbitrarily shaped three-dimensional shaped structures. *Geophysics* **44**, 753–780.

Edwards L.S. 1977. A modified pseudosection for resistivity and induced-polarization. *Geophysics* **42**, 1020–1036.

Eisenstat S.C., Schultz M.H. and Sherman A.H. 1976. Considerations in the design of software for sparse Gaussian elimination. In: *Sparse Matrix Computations* (eds J.R. Bunch and D.J. Rose), pp. 427–438. Academic Press, Inc.

George A. and Liu J.W. 1981. *Computer Solution of Large Sparse Positive Definite Systems*. Prentice–Hall, Inc.

Golub G.H. and van Loan C.F. 1989. *Matrix Computations*. The Johns Hopkins University Press.

Griffiths D.H. and Barker R.D. 1993. Two-dimensional resistivity imaging and modelling in areas of complex geology. *Journal of Applied Geophysics* **29**, 211–226.

Griffiths D.H., Turnbull J. and Olayinka A.I. 1990. Two-dimensional resistivity mapping with a computer-controlled array. *First Break* **8**, 121–129.

Koefoed O. 1979. *Geosounding Principles 1: Resistivity Sounding Measurements*. Elsevier Science Publishing Co.

Li Y. and Oldenburg D.W. 1992. Approximate inverse mappings in DC resistivity problems. *Geophysical Journal International* **109**, 343–362.

Lines L.R. and Treitel S. 1984. Tutorial: A review of least-squares inversion and its application to geophysical problems. *Geophysical Prospecting* **32**, 159–186.

Loke M.H. and Barker R.D. 1995. Least-squares deconvolution of apparent resistivity pseudosections. *Geophysics* 60, 1682–1690.

Loke M.H. and Barker R.D. 1996. Rapid least-squares inversion of apparent resistivity pseudosections using a quasi-Newton method. *Geophysical Prospecting* 44, 131–152.

Martin R.S. and Wilkinson J.H. 1965. Symmetric decomposition of positive definite band matrices. *Numerische Mathematik* 7, 355–361.

Mooney H.M., Orellana E., Pickett H. and Tornheim, L. 1966. A resistivity computation method for layered earth models. *Geophysics* **31**, 192–203.

Park S.K. and Van G.P. 1991. Inversion of pole-pole data for 3-D resistivity structures beneath arrays of electrodes. *Geophysics* **56**, 951–960.

Petrick W.R. jr., Sill W.R. and Ward S.H. 1981. Three-dimensional resistivity inversion using alpha centers. *Geophysics* **46**, 1148–1163.

Press W.H., Flannery B.P., Teukolsky S.A. and Vetterling W.T. 1988. *Numerical Recipes in C*. Cambridge University Press.

Sasaki Y. 1989. Two-dimensional joint inversion of magnetotelluric and dipole-dipole resistivity data. *Geophysics* **54**, 254–262.

Sasaki Y. 1994. 3-D resistivity inversion using the finite-element method. *Geophysics* **59**, 1839–1848.

Shima H. 1992. 2-D and 3-D resistivity image reconstruction using crosshole data. *Geophysics* 57, 1270–1281.

Woo P.T., Eisenstat S.C., Schultz M.H. and Sherman A.H. 1976. Application of sparse matrix techniques to reservoir simulation. In: *Sparse Matrix Computations* (eds J.R.Bunch and D.J. Rose), pp. 427–438. Academic Press, Inc.

Xu B. and Noel M. 1993. On the completeness of data sets with multielectrode systems for electrical resistivity survey. *Geophysical Prospecting* **41**, 791–801.